Received: 25 August 2021 | Revised: 10 May 2022 | Accepted: 26 August 2022

DOI: 10.1002/jnm.3066

SPECIAL ISSUE PAPER

WILEY

Eddy current loss estimation for direct drive wind turbine generators with superconducting excitation winding by numerical and analytical models

Robin Köster | **Andreas Binder**

Department of Electrical Engineering and Information Technology, Institute of Electrical Energy Conversion, Technical University Darmstadt, Darmstadt, Germany

Correspondence
Robin Köster, Department of Electrical Engineering and Information Technology, Institute of Electrical Energy Conversion, Technical University Darmstadt, Landgraf-Georg-Straße 4, Darmstadt 64287, Germany.
Email: rkoester@ew.tu-darmstadt.de

Funding information
Stiftung Energieforschung Baden-Württemberg

Abstract

Direct drive wind turbine generators with superconducting excitation winding are studied with focus on the electromagnetic damper design. A semi-analytical eddy current model is built for parametric design studies based on a vector potential approach. The considered generators employ open stator slots and exhibit strong saturation effects, so that an analytical expression for the source terms is not adequate. Whilst the field equations are solved analytically, an equivalent current loading, accounting for slotting effects and saturation, is obtained by magnetostatic models applying the 2D finite element method (FEM). The proposed framework for the extraction of the current loading is universal and may also be applied to other machine types (e.g., permanent magnet synchronous machines, [PMSM]). In relation to transient FEM models, a considerable time-saving can be achieved, which is particularly beneficial in case of large models, for example, in case of fractional slot windings or intermittent feeding schemes. The eddy current loss in warm and cold rotor parts in a direct drive generator in the 7 MW power class are computed with the semi-analytical and transient 2D FEM models under variation of the damper geometry and the stator winding configuration. Minimum damper dimensions as well as constraints regarding applicable stator windings are derived.

KEYWORDS

damper design, direct drive generators, eddy current loss, electrical machine, finite element method, superconducting excitation

1 | INTRODUCTION

Large direct drive wind turbine generators (≥7 MW) abandon the gear and the corresponding maintenance at the cost of a strong increase in generator size and material usage (slab-like designs). Recent developments, especially in the market for offshore applications, are characterised by an ever increasing rated unit power. One limitation of this

trend consists in the restricted installation space for the electric generator as well as in the mass located in the nacelle. Direct drive solutions generally also exhibit a lower efficiency than high speed generator designs.[1] Commercially available direct drive generators are nowadays excited by permanent magnets (PMs), which restrict efficiency and torque density from a cost-oriented perspective in regards to the material usage. In this context, high temperature superconducting (HTS) excitation windings may allow for more compact generator designs,[2] which come along with higher overall efficiency (∼95%), larger power factor and reduced costs for constructive measures. The excitation windings require long tape lengths ($l \sim 500$ m), which are to this date still rather expensive ($p' \sim 80...100$ EUR/[kA m]). Moreover, the HTS excitation technology competes with the well-established PM excitation,[3] so that generator designs with minimum usage of HTS material are most promising. This requirement implies ferromagnetic rotor parts, a stator winding in slots and stator winding configurations with maximum fundamental winding factor $k_{w,1}$.

The pole pair of an exemplary HTS generator is shown in Figure 1. Employing a cold rotor iron is in favour of a simpler cryostat design and improves the thermal stability. In spite of the large effective air gap width, the proximity to ferromagnetic parts, which determines the local magnetic field conditions of the HTS excitation winding, and the possibly large content of stator field harmonics imply the requirement for an electromagnetic damper screen, which is attached to the cryostat wall.[2]

A suitably designed damper screen ensures a reduction of AC loss in the HTS winding to sufficiently low values, protects the field winding from overcurrents, improves the generator's transient stability and leads to a reduction of the eddy current loss in massive cold rotor parts, which must be removed by the cryogenic cooling system. These requirements must be fulfilled by also limiting the loss in warm parts (cryostat wall, damper) at nominal operation. From these requirements, this work focuses on the eddy current loss in cold and warm parts. In order to prevent additional complexity, a simple forced air cooling of the damper and the cryostat wall is most suitable. This limits the admissible loss due to the heat transfer restrictions and leads to the requirement to ensure a sufficiently low temperature at the warm side of the multi-layer insulation (MLI) equipped heat flux path to the cold rotor parts.

The computation of the eddy current loss in large finite element method (FEM) models is however time consuming, already in case of 2D models: Free eddy currents pose challenges in terms of sufficiently fine meshs, short time steps and long settling times. Preliminary design considerations require therefore a fast alternative, which accounts for all relevant effects. Results from magnetostatic 2D FEM models without eddy current reaction may therefore serve as input for a fast, analytical eddy current loss model.

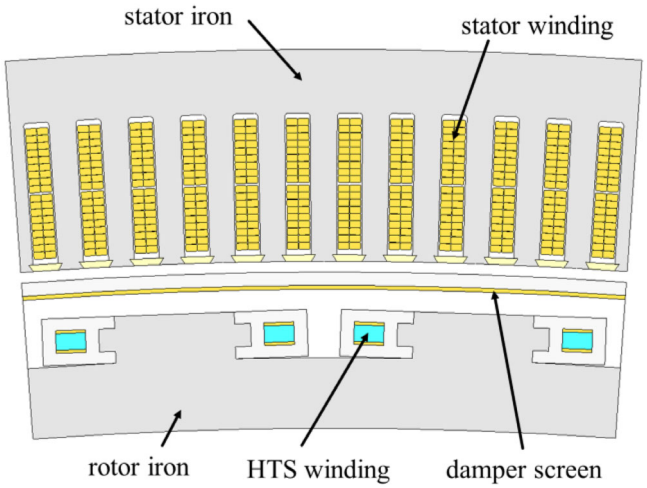

FIGURE 1 Model section covering one pole pair of the high temperature superconducting (HTS) generator. The 2D finite element method model is set up with the software JMAG 20. The considered HTS generator design employs a cold rotor yoke and cold pole cores as wel a conventional stator winding in slots.

2 | SEMI-ANALYTICAL EDDY CURRENT MODEL OF HTS GENERATORS

This section is on the semi-analytical electro-magnetic field model, which allows for the computation of theddy current loss in cold and warm parts by accounting for the cylindrical geometry. The analytical computations are implemented in MATLAB whereas the magnetostatic 2D FEM simulations are set up with the free software FEMM.[4]

2.1 | Analytical electromagnetic field model

The analytical electro-magnetic field model is based on the vector potential approach and assumes translational invariance in z-direction: $\partial_z A_z \equiv \partial A_z/\partial z = 0, \forall z$. The model is rotationally symmetric implying the use of polar coordinates r, γ (in mechanical degrees). This simplification implies only approximate results but is justified for the following reasons:

1. The stator slotting is incorporated by using an equivalent current loading that is obtained by a FEM simulation with a slotted stator structure.
2. The rotor poles are highly saturated by the fundamental of the main flux. From a simplified air-gap field harmonics' perspective, there is only a small variation ($\mu_r = 1...10$) of reluctance in circumferential direction.
3. For the considered stator winding configurations, the wave lengths of air-gap field harmonics is small compared to typical pole dimensions. This allows for a simple scaling by the pole width of the computed eddy current loss in the pole region during a subsequent step.

A generalisation to a model without rotational symmetry is discussed below, but comes along with a higher computational effort, which is not justified for the considered application. The model involves 9 regions and is shown in Figure 2. A generalisation to less/more regions is straight-forward as shown by Anglada et al.[5] The constituting field equations are solved for each region separately, whilst the continuity relations for the normal component of the flux density B_r and the tangential component of the magnetic field strength H_γ fix the remaining degrees of freedom. The low frequencies in the order of $f \sim 5$ Hz (fundamental)...150 Hz (relevant harmonics) allow to neglect any displacement currents. The model assumes linear material properties, which represents a major disadvantage of the analytical computation. Saturation effects are however partially contained in the equivalent current loading.

Combining Faraday's law of induction and Ampére's law yields (1) (SI units). The source term is represented by the current loading at the stator bore and consequently enters via the continuity relations. The translational symmetry implies a current loading $\vec{K}$ with out-of-plane orientation: $\vec{K} = K \cdot \vec{e}_z$. This translates to $\vec{E} = E_z \cdot \vec{e}_z$ and $\vec{A} = A_z \cdot \vec{e}_z$.

$$\nabla \times \left(\mu^{-1} \cdot \nabla \times \vec{A}\right) = -\kappa \cdot \partial_t \vec{A} \tag{1}$$

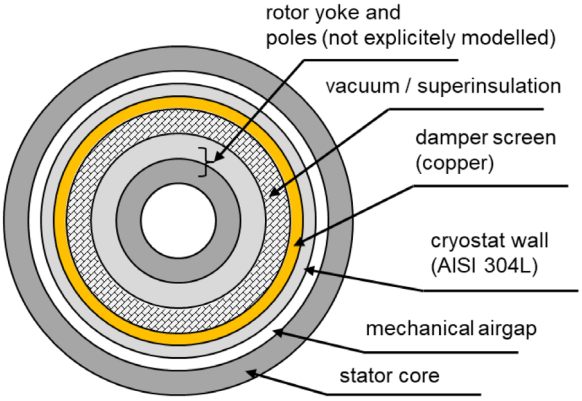

FIGURE 2 Schematic visualisation of the equivalent generator model for the computation of the eddy current loss in cold and warm rotor parts. The assigned material properties are listed in Table 1.

Without loss of generality, the current loading can be represented by its two-dimensional Fourier transform (2) where δ(r) denotes the Dirac delta function and $\omega = 2\pi f_s$ is the electrical angular frequency. The spectral domain is spanned by the absolute space order ν (fundamental: $\nu = p$) and time order k.

$$K_z(r,\gamma,t) = \sum_{\nu}\sum_{k} \underline{K}_{\nu,k} \cdot \delta(r - r_{si}) \cdot e^{j} \cdot (\nu \cdot \gamma + k \cdot \omega \cdot t) \tag{2}$$

The time harmonic excitation (2) implies also a time harmonic evolution of all field quantities according to (3). The superscript n refers to quantities in region n.

$$A_z^n(r,\gamma,t) = \sum_{k} \underline{A}_{z,k}^n(r,\gamma) \cdot e^{jk\omega t} \tag{3}$$

By using the coulomb gauge $\nabla \cdot \vec{A} = 0$, the Helmholtz equation (4) for contributions of time order k can be derived. In case of rotating regions, the effective time order k must be used.

$$\Delta \underline{A}_{z,k}^n(r,\gamma) - j \cdot k\omega\mu^n\kappa^n \cdot \underline{A}_{z,k}^n(r,\gamma) = 0 \tag{4}$$

The separation of variables implies an ansatz as series of harmonics according to (5).

$$A_{z,k}^n(r,\gamma) = \sum_{\nu} \underline{R}_{\nu,k}^n(r) \cdot e^{j \cdot \nu \cdot \gamma} \tag{5}$$

Inserting this ansatz in (4) yields (6). Here, we give the general expression that allows for a variation of the conductivity κ in circumferential direction (e.g., highly saturated poles separated by pole gaps or surface-mounted PMs).

$$\sum_{\nu}\left[\partial_r^2 \underline{R}_{\nu,k}^n(r) + \frac{1}{r} \cdot \partial_r \underline{R}_{\nu,k}^n(r) - \frac{\nu^2}{r^2} \cdot \underline{R}_{\nu,k}^n(r)\right] \cdot e^{j\nu\gamma} - j \cdot k\omega\mu^n \cdot \sum_{\nu,\nu'} \underline{\kappa}_{\nu'}^n \cdot \underline{R}_{\nu',k}^n(r) \cdot e^{j(\nu+\nu')\gamma} = 0 \tag{6}$$

Equating coefficients of equal phase leads to a system of coupled differential equations, which can be written by using matrix notation (7). Here, $\underline{\underline{N}}^n$ is a diagonal matrix whereas $\underline{\underline{M}}^n$ contains off-diagonal coupling terms. The diagonalisation of the coupling matrix is straight-forward and leads to equivalent equation systems but is not within the scope of this work. It may, however, widen the field of application, if the aforementioned simplifications are not justified.

$$\partial_r^2 \underline{\vec{R}}^n + \frac{1}{r} \cdot \partial_r \underline{\vec{R}}^n - \left[\frac{1}{r^2} \cdot \underline{\underline{N}}^n + \underline{\underline{M}}^n\right] \underline{\vec{R}}^n = 0 \tag{7}$$

In case of constant conductivity in all regions, there is no coupling and the differential equation in the form (8) can be solved for each space order ν separately. These equations are solved by (9), where $\underline{I}_\nu$ and $\underline{K}_\nu$ are the modified Bessel functions of first and second kind with order ν.

$$\partial_r^2 \underline{R}_{\nu,k}^n(r) + \frac{1}{r} \cdot \partial_r \underline{R}_{\nu,k}^n(r) - \left[\frac{\nu^2}{r^2} + j \cdot k\omega\mu^n\kappa^n\right] \cdot \underline{R}_{\nu,k}^n(r) = 0 \tag{8}$$

$$\underline{R}_{\nu,k}^n(r) = \begin{cases} \underline{C}_{\nu,k}^n \cdot \underline{I}_\nu\left(\underline{\vartheta}_k^n r\right) + \underline{D}_{\nu,k}^n \cdot \underline{K}_\nu\left(\underline{\vartheta}_k^n r\right), & \text{for } \kappa_n \neq 0 \\ \underline{C}_{\nu,k}^n \cdot r^\nu + \underline{D}_{\nu,k}^n \cdot r^{-\nu}, & \text{for } \kappa_n = 0 \end{cases} \tag{9}$$

The coefficients $\underline{C}_{\nu,k}^n$, $\underline{D}_{\nu,k}^n$ are fixed by continuity and boundary conditions (finite field quantities for $r \to 0$ and $r \to \infty$), whereas the parameter $\underline{\vartheta}_k^n$, (10), determines the penetration into the respective conductive region. Again, the time order that is effective in region n must be used.

$$\underline{\vartheta}_k^n = \sqrt{j \cdot k\omega\mu^n\kappa^n} \tag{10}$$

TABLE 1 Material properties in the analytical electromagnetic field model

	κ/(MS/m)	μ_r
Stator core	0	1000
Air gap	0	1
Cryostat wall (AISI 304 L)	1.31	1
Damper (Cu, $\vartheta = 70°C$)	48.15	1
MLI	0	1
Pole region (FeNi9, $T = 30$ K)	8.268	1
Rotor yoke (FeNi9, $T = 30$ K)	8.268	1000
Interior (Air)	0	1

Abbreviation: MLI, multi-layer insulation.

The preceding set of equations results in a linear system of equations for the coefficients $\underline{C}^{\mathrm{n}}_{\nu,\mathrm{k}}$, $\underline{D}^{\mathrm{n}}_{\nu,\mathrm{k}}$. Field quantities can be derived from the vector potential, e.g., the magnetic flux density (11) entering the continuity conditions.

$$B^{\mathrm{n}}_{\gamma}(r,\gamma,t) = -\partial_r A^{\mathrm{n}}_{\mathrm{z}}(r,\gamma,t) = -\sum_{\nu}\sum_{\mathrm{k}}\left(\partial_r \underline{R}^{\mathrm{n}}_{\nu,\mathrm{k}}(r)\right)\cdot e^{\mathrm{j}\cdot(\nu\cdot\gamma+k\cdot\omega\cdot t)} \tag{11a}$$

$$B^{\mathrm{n}}_{r}(r,\gamma,t) = \frac{1}{r}\cdot\partial_\gamma A^{\mathrm{n}}_{\mathrm{z}}(r,\gamma,t) = \sum_{\nu}\sum_{\mathrm{k}}\mathrm{j}\frac{\nu}{r}\cdot\underline{R}^{\mathrm{n}}_{\nu,\mathrm{k}}(r)\cdot e^{\mathrm{j}\cdot(\nu\cdot\gamma+k\cdot\omega\cdot t)} \tag{11b}$$

The time-averaged power transfer in radial direction is determined by means of the Poynting vector $\vec{S} = \vec{E}\times\vec{H}$ according to (12). The eddy current loss in region n is determined by subtraction of in-flow and out-flow power at the region boundaries.

$$\overline{P}^{\mathrm{n}}_{\mathrm{Ft}}(r) = f_{\mathrm{s}}\cdot\int_0^{1/f_{\mathrm{s}}}\mathrm{dt}\int_0^{2\pi} r\mathrm{d}\gamma\int_0^{L}\mathrm{dz}S^{\mathrm{n}}_{r}(r,\gamma,t) = -2\pi\cdot L\cdot r\cdot\frac{k\omega}{\mu^{\mathrm{n}}}\sum_{k}\sum_{\nu}\mathrm{Im}\left\{\underline{R}^{\mathrm{n}}_{\nu,\mathrm{k}}(r)\cdot\left(\partial_r\underline{R}^{\mathrm{n}}_{\nu,\mathrm{k}}(r)\right)^{*}\right\} \tag{12}$$

MATLAB allows to solve the resulting system of equations either by means of symbolic variables or by applying numerical schemes. The latter come along with a huge time-saving and are therefore used in this study. Still, the implementation may face challenges regarding numerical stability in case of large absolute values of space order $|\nu|$ and large generator diameters.

The material properties used for the analytical model are listed in Table 1. The high relative permeability of stator yoke ensures that the correct tangential field H_γ is impressed by means of the equivalent current loading K. The chosen permeability of the rotor yoke is based on the assumption of moderate saturation in this flux path section and has only minor influence on the eddy current loss. The temperatures of the cold rotor yoke and poles are chosen in accordance with a reasonable range of the HTS op temperature. It should be mentioned, that a complete description of the eddy current model requires a three-dimensional model setup, which is not within the scope of this work. It rather aims for a fast eddy current model suited for parameter studies, from which qualitative and, within some tolerance, quantitative results can be drawn. 3D effects are incorporated in the study by adjusting the conductivity values listed in Table 1 by end-effect factors to an approximate effective value.[6]

2.2 | Determination of the equivalent current loading

The air gap field harmonics, causing the eddy current loss, comprise both stator field harmonics and rotor field modulations due to the slotted stator. In this sense, the origin of harmful field harmonics is geometrically located at the stator inner surface. To approximately reproduce the field configuration in the analytical model, it is suitable to impress the tangential magnetic field strength H_γ at the stator bore. For a sufficiently large stator permeability (13) holds.

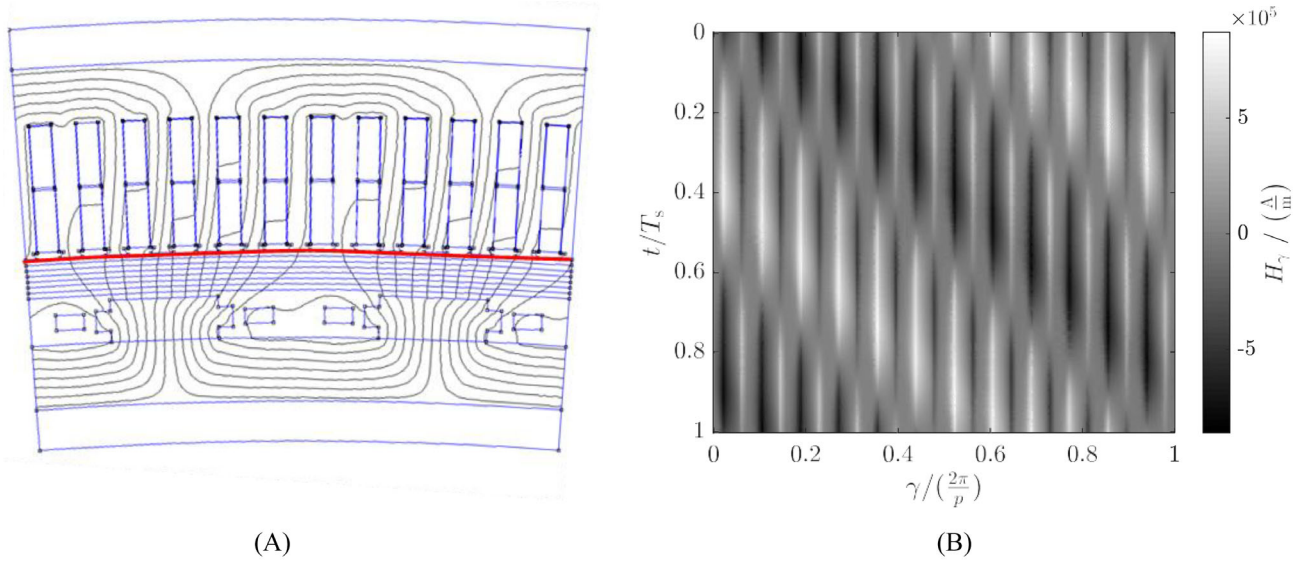

FIGURE 3 (A) 2D finite element method model of the high temperature superconducting generator built in FEMM with evaluation contour in red, (B) two dimensional (time t, circumferential angle γ_{el}) representation of the tangential component of the magnetic field strength $H_\gamma(\gamma, t)$, stator winding: $q = 2$, $W/\tau_p = 5/6$ (Stator reference frame)

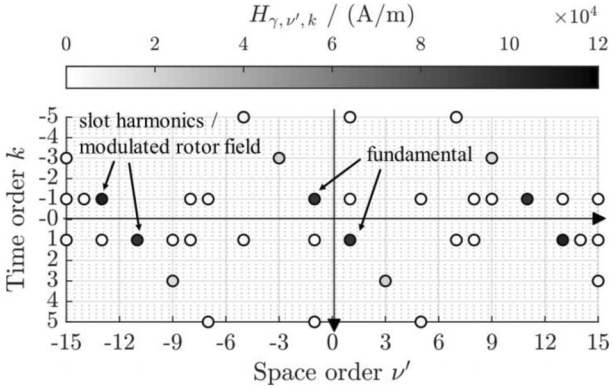

FIGURE 4 2D spectral representation of the magnetic field strength tangential component H_γ at the stator bore. The component H_γ corresponds to the impressed current loading in the analytical eddy current model, where $k = 1$ corresponds to a time evolution with electrical frequency f_s. Stator winding: $q = 2$, $W/\tau_p = 5/6$ (stator reference frame)

$$H_\gamma\left(r = r_{si}^-, \gamma, t\right) = K_z(r = r_{si}, \gamma, t) \tag{13}$$

The component H_γ is extracted from a series of magnetostatic 2D FEM simulations with the free software FEMM. An exemplary model together with the magnetic flux lines at nominal operation are shown in Figure 3A for a short-pitched stator winding with $q = 2$, $W/\tau_p = 5/6$. The magnetostatic model comprises an entire winding scheme corresponding to $\gamma_{el} = 2\pi$. Several simulations for N_t time steps (e.g., $N_t = 201$) within one fundamental period $T_s = 1/f_s$ are carried out, where the rotor is successively moved. The tangential field is evaluated along the red contour and is visualised in Figure 3B in a two-dimensional representation (stator reference frame). The moving stator poles as well as the stationary modulation due to the stator slotting can be observed.

A 2D discrete Fourier transform yields the corresponding spectral representation,[7] which is shown in Figure 4. This spectrum is related to the one of the current loading $\underline{K}_{\nu,k}$ via (13). An analytical approach for the stator current loading, for example, following Štěpina,[8] would yield the well-known spectrum with contributions for relative space orders

$|\nu'| = 1, 5, 7, 11, 13, 17, 19, \ldots$ and time order $|k| = 1$. Here, the combination of signs of space and time order determines the sense of rotation, where for example the combinations $\{\nu' = +5, k = -1\}$ and $\{\nu' = -5, k = +1\}$ together represent one air gap field harmonic. The slot opening as well as saturation effects lead to additional harmonic contributions. Harmonics with $\nu' = k$ rotate, however, synchronously without contribution to the eddy current loss, whereas the contribution by field harmonics like $\{\pm 9, \mp 3\}$ would not be covered by a model which includes entirely analytical current loading source terms.

As the eddy current reaction is neglected in the first step, the Fourier coefficients $\underline{K}_{\nu,k}$ must just be determined once, if several damper geometries should be studied. Different dampers with accordingly varying eddy current reaction are hence subject to an air gap field that is excited by the same current loading. This approximation is based on the assumption that the eddy current reaction field at the stator bore is much smaller than the field harmonics that give rise to eddy currents flowing in the rotating parts.

2.3 | Considered HTS generator design

The main data of the considered HTS generator designs is listed in Table 2. Based on the required output power and stator nominal voltage, the current angle, the excitation current I_f, the number of turns of the excitation winding N_f and the number of turns per phase N_s (stator) are adjusted by following an iterative procedure.[9]

Different stator winding configurations contribute to the eddy current loss in three ways:

1. The number of slots per pole per phase q and the pitching W/τ_p directly determine the content of stator field harmonics.
2. The winding factor of the fundamental, torque-producing field wave $k_{w,\nu}{}' = 1$ determines the required rotor field for constant output power. The rotor field is modulated by the permeance modulation of the slotted stator, so that a higher rotor field increases the eddy current loss considerably.
3. The number of slots per pole per phase q influences the spectrum of the permeance modulation (open slots with slot opening s_Q) with regard to occurring harmonics as well as to their amplitude. This effect is especially important as the distance from the stator bore to the cryostat wall should be small from a cost-oriented perspective (required HTS material).

The operating temperature of the HTS excitation winding is chosen as $T_{SC} = 30$ K in order to ensure a sufficiently high utilisation of the HTS material. A thermal model of the cryogenic parts yields temperatures of the cold rotor yoke and of the rotor poles that differ slightly from the target temperature with only minor influence on the magnetic and electric properties affecting the eddy current loss.

TABLE 2 Fixed high temperature superconducting generator data serving as input for the iterative design process.

Fixed HTS generator data serving as input for the iterative design process		
P_N	MW	7
U_N	V	690
I_N	A	6180
$\mathrm{Cos}(\varphi_N)$	—	0.95
n_N	rpm	10
f_N	Hz	7.33
m_s	—	3
$2p$	—	88
d_{so}	mm	6691
L	mm	1137.5
δ_{geom}	mm	8

2.4 | Comparison to 2D FEM simulation results

The eddy current density in the cryostat wall and the damper screen is visualised in Figure 5B in case of a stator winding with $q = 1$, $W/\tau_p = 1$ for one pole pair. This stator winding gives rise to a maximum content of air gap field harmonics for a clear visualisation. The transient FEM simulation runs for several hours, whereas the semi-analytical model provides results within less than 5 min on the same machine, corresponding to a time saving by a factor in the order of ∼50...100.

The semi-analytical model yields an eddy current distribution in warm parts that agrees qualitatively and quantitatively well to the results of the transient 2D FEM simulation. Pronounced eddy current waves with relative space orders $\nu' = \nu/p = \pm 5, \pm 7$ in the damper and the cryostat wall can be observed:

1. The localisation of the coil sides in slots gives rise to slot harmonics with lowest relative space orders $\nu' = \pm 5, \pm 7$. (Combinations: $\{\nu' = \pm 5, k = \mp 1\}$, $\{\nu' = \pm 7, k = \pm 1\}$ in stator reference frame)
2. The rotor field with fundamental of orders $\nu' = \pm 1$, $k = \pm 1$ (synchronous rotation) is modulated by a permeance function $\lambda(\gamma)$ with 6 periods per winding scheme, yielding prominent air gap field harmonics according to (14).

$$\begin{aligned} \underline{B}^{(\mathrm{R})}_{\sim} &= \left[\underline{B}_{+1,+1} \cdot e^{j(\gamma+\omega t)} + \underline{B}_{-1,-1} \cdot e^{-j(\gamma+\omega t)}\right] \cdot \left[\underline{\lambda}_{+6,0} \cdot e^{j6\gamma} + \underline{\lambda}_{-6,0} \cdot e^{-j6\gamma}\right] \\ &= \underbrace{\underline{B}^{(\mathrm{R})}_{+1,+1} \cdot \underline{\lambda}_{+6,0}}_{=: \underline{B}_{\sim,+7,+1}} \cdot e^{j(7\gamma+\omega t)} + \underbrace{\underline{B}^{(\mathrm{R})}_{-1,-1} \cdot \underline{\lambda}_{-6,0}}_{=: \underline{B}_{\sim,-7,-1}} \cdot e^{-j(7\gamma+\omega t)} + \underbrace{\underline{B}^{(\mathrm{R})}_{+1,+1} \cdot \underline{\lambda}_{-6,0}}_{=: \underline{B}_{\sim,-5,+1}} \cdot e^{j(-5\gamma+\omega t)} + \underbrace{\underline{B}^{(\mathrm{R})}_{-1,-1} \cdot \underline{\lambda}_{+6,0}}_{=: \underline{B}_{\sim,+5,-1}} \cdot e^{j(5\gamma-\omega t)} \end{aligned} \tag{14}$$

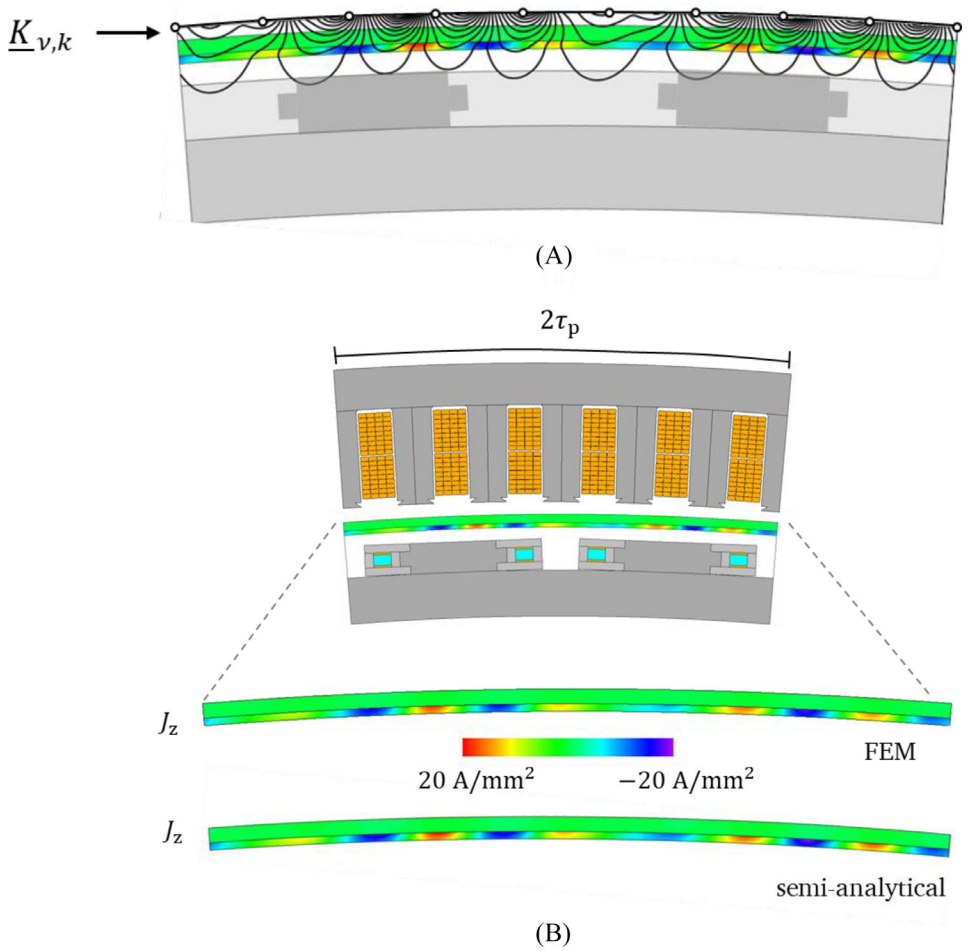

FIGURE 5 (A) Analytically computed flux lines of air gap field harmonics for a stator winding with $q = 1$, $W/\tau_p = 1$ based on the eddy current calculation. The rotor poles are not explicitly modelled but visualised for a better understanding. (B) Comparison of the corresponding eddy current distribution in the damper screen and the cryostat wall for the 2D finite element method (FEM) model i0mplemented in JMAG 20 (top) and the semi-analytical model (bottom).

The eddy current loss induced by the modulation of the rotor field fundamental constitutes a major contribution to the overall eddy current loss, which is already present at no-load operation. This effect can be attributed to the high rotor field in HTS generators and to the open stator slots. The choice of sufficiently high q constitutes the reasonable measure to cope with this loss component in spite of the marginally increasing rotor field. The dominant harmonics with space orders $\nu' = \pm 5, \pm 7$ are considerably less pronounced in the spectrum for the short-pitched winding with doubled number of slots ($q = 2$, $W/\tau_p = 5/6$), Figure 4.

The semi-analytically computed field lines for the stator winding with $q = 1$, $W/\tau_p = 1$ are visualised in Figure 5A for a thickness of the cryostat wall $d_{\text{cryostat wall}} = 10$ mm (fulfilling mechanical requirements) and a damper thickness of $d_{Cu} = 3$ mm. The course of the flux lines shows that only harmonics with the longest wave length just reach the rotor pole surface, which justifies the truncation of the series over space orders ν. However, since even small eddy current loss in cold iron parts must be avoided, the stator winding with $q = 1$, $W/\tau_p = 1$ (providing $k_{w,1} = 1$) proves infeasible in spite of the large effective air gap.

Similar agreement of the semi-analytical model and transient 2D FEM simulations are also observed for all other considered fractional and integer slot windings. As an example, a quantitative comparison for the eddy current loss in the cold parts is visualised in Figure 6A for a $q = 2$, $W/\tau_p = 1$ stator winding. The damper thickness d_{Cu} is varied for constant effective air gap width (distance between stator bore and outer pole radius) and constant thickness of the cryostat wall $d_{\text{cryostat wall}} = 10$ mm. The semi-analytical model correctly predicts the overall loss. To account for the pole cores, the eddy current loss in the (simplified, cylindrically symmetric) pole section of the semi-analytical model is scaled by the factor w_p/τ_p, where w_p denotes the poles' width. This simple scaling is justified by the aforementioned circumstances arising from the considered windings and the highly saturated pole core. In particular, the semi-analytical model correctly reproduces the dependence on the damper screen's thickness, which shows a strong decrease of the eddy current loss in cold parts towards large d_{Cu}. For the considered design, the maximum thickness of the screen is in the order of $d_{Cu} \sim 10...12$ mm to accommodate the MLI.

The eddy current loss in the warm damper screen and the cryostat wall is shown in Figure 6B. A slight overestimation by the semi-analytical model can be observed, which is attributed to the neglect of the direct eddy current reaction and to the simplifications regarding the model geometry. The eddy current loss in the cryostat shows only minor changes under variation of d_{Cu}, whereas the loss in the damper screen shows a strong increase as notable shielding of the cold rotor sets in. Due to the low fundamental frequency $f_s = 7$ Hz the skin depth in the copper damper is in the order of $d_E \sim 11$ mm for the dominant field harmonics with time order $k = 6$ (rotor reference frame, $\nu' = \pm 5, \pm 7$) and $d_E \sim 8$ mm for $k = 12$ (rotor reference frame, $\nu' = \pm 11, \pm 13$) respectively. The improved shielding (low $P_{\text{Ft,cold}}$) is therefore accompanied by only minor changes in $P_{\text{Ft,warm}}$ as d_{Cu} increases.

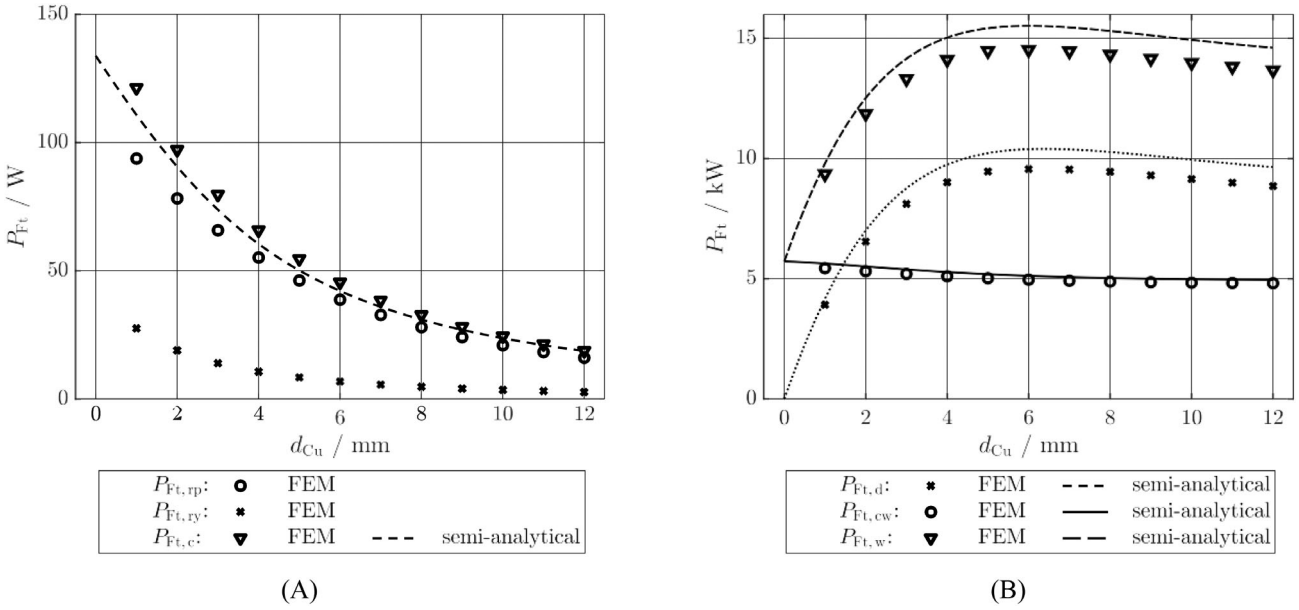

FIGURE 6 Comparative visualisation of the additional loss in the rotor cold parts (A) and the warm parts (B) under variation of the damper thickness d_{Cu} for a stator winding with $q = 2$, $W/\tau_p = 1$. Results are shown for the 2D transient finite element method (FEM) model (JMAG 20) and the semi-analytical model.

3 | PARAMETER STUDY OF DAMPER DESIGNS

This section is on a parameter study of the influence of the damper design on the eddy current loss in warm and cold parts of the HTS generator specified in Section 2.3. Considered parameters are the thickness of the copper damper d_{Cu}, the cryostat wall $d_{\mathrm{cryostat\ wall}}$ as well as the stator winding configuration, characterised by the number of slots per pole per phase q and the pitching ratio W/τ_{p}.

3.1 | Eddy current loss in the damper screen and cryostat wall

The eddy current loss in the damper screen under variation of the cryostat wall thickness $d_{\mathrm{cryostat\ wall}}$ is shown in Figure 7A. The number of slots per pole per phase is restricted by requiring that the slot pitch must not become too small for a given stator bore diameter. The considered stator windings comprise integer slot windings ($q = 1$, $q = 2$, $q = 3$) with a fundamental $\nu' = 1$ and a wave length $\lambda_1 = 2\tau_{\mathrm{p}}$. In addition, fractional slot windings are studied, where the denominator of q is restricted to 2. This prevents the occurrence of sub-harmonics with $\nu < p$ and wave lengths $\lambda_\nu > 2\tau_{\mathrm{p}}$, which more easily reach the cold rotor and build up a larger magnetic flux, inducing eddy currents.[10]

The damper loss strongly depends on the thickness of the cryostat wall $d_{\mathrm{cryostat\ wall}}$ for two reasons:

1. The stainless steel cylinder yields some stronger screening as $d_{\mathrm{cryostat,wall}}$ is increased. Owing to the rather low conductivity, this effect has only minor influence on $P_{\mathrm{Ft,damper}}$.
2. The dominant effect arises from the increasing distance between the origin of air gap field harmonics and the copper screen. In contrast, the eddy current loss in cold rotor parts is nearly unchanged under variation of $d_{\mathrm{cryostat\ wall}}$. This is attributed to harmonics with comparably high space order ν, which cause additional loss in the damper screen,[11] whereas they do not reach the cold rotor iron owing to their short wave length $\lambda_\nu \sim \nu^{-1}$. This holds even in case of thin copper screens or even without additional damper. Consistently, a similar decrease of the loss in the damper for the windings with $q = 2$ and with or without pitching can be observed in Figure 7A. The short pitched winding nearly lacks of harmonics of space orders $|\nu'| = 5, 7$ whereas the slot harmonics as well as the harmonics caused by the rotor field modulation remain unchanged ($|\nu'| = 11, 13$) apart from small changes in the generator's excitation.

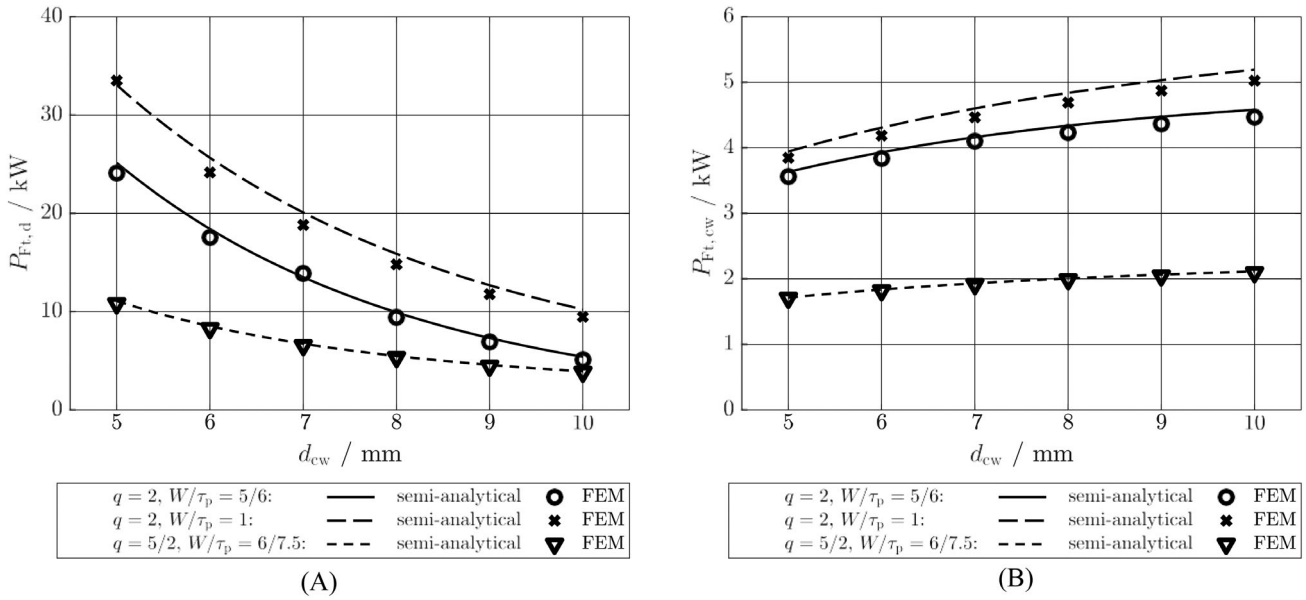

FIGURE 7 Visualisation of the eddy current loss in the copper damper screen (A) and the cryostat wall (B) under variation of the cryostat wall's thickness. Results are shown for the 2D transient finite element method (FEM) model (JMAG 20, symbols) and the semi-analytical model (lines).

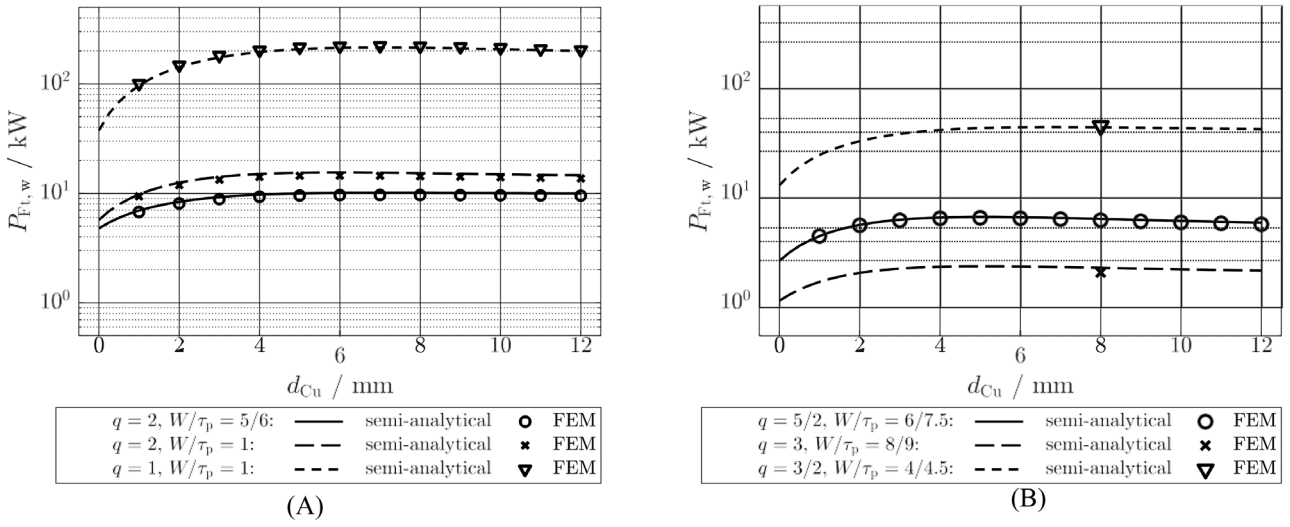

FIGURE 8 Visualisation of the eddy current loss in the warm rotor parts (copper damper and cryostat wall) under variation of the copper damper's thickness d_{Cu} for different stator winding configurations (A), (B). Results are shown for the 2D transient finite element method (FEM) model (JMAG 20) and the semi-analytical model.

The loss in the stainless steel cryostat wall (Figure 7B) shows a slight increase towards larger values of $d_{\mathrm{cryostat\ wall}}$. Due to the low conductivity, the skin depth is in the order of $d_{\mathrm{E}} \sim 67$ mm for $|\nu'| = 5, 7$ ($k = 6$ in rotor reference frame) and $d_{\mathrm{E}} \sim 48$ mm for $|\nu'| = 11, 13$ ($k = 12$ in rotor reference frame). The large values of d_{E} compared to $d_{\mathrm{cryostat,wall}}$ imply only a slight decrease of the field and the current density over the cylinder's thickness. This corresponds to a quite uniform loss density P_{Ft} in radial direction, so that an increase in wall thickness mainly manifests in a larger volume that is subject to the eddy current loss.

A variation of the copper screen thickness yields the eddy current loss in warm parts, shown in Figure 8 at a logarithmic scale. The additional loss varies by up to two orders of magnitude for the same outer dimensions of the HTS generator and the same geometry of the cryostat wall and the damper. Since efficiency is a crucial design criterion for large wind turbine generators, an admissible additional loss is in the order of ∼0.25% of the rated power. This corresponds to around $P_{\mathrm{Ft,warm}} \sim 10...20$ kW for the considered HTS generators, Section 2.3. Figure 8 reveals that this requirement can only be met by integer slot windings, where $q \geq 2$ or by the short pitched fractional slot winding $q = 5/2$. This holds even in case of a maximum damper screen thickness. The disadvantage of small slot numbers per pole per phase is attributed to the strong contribution by the modulated rotor field and represents, together with manufacturability requirements, an upper limit on the generator's pole count.

3.2 | Eddy current loss in cold parts

The heat load in the cold parts directly enters both the overall efficiency and, by the capacity of the cooling system, the HTS generator's overall cost. Besides the heat leakage, any additional loss dissipation must be kept at a minimum. In view of typical coefficients of performance in the order of ∼1...1.5% at $T = 30$ K, the eddy current loss in cold parts should not exceed values around $P_{\mathrm{Ft,cold}} \sim 50$ W. The eddy current loss in cold parts for all considered stator windings is visualised in Figure 9 under variation of the damper thicknes d_{Cu}. The decrease of $P_{\mathrm{Ft,cold}}$ varies considerably amongst the windings, where the damping is the strongest for $q = 2$, $W/\tau_{\mathrm{p}} = 5/6$ leading to a reduction by about one order of magnitude. The restrictions on the maximum admissible value of $P_{\mathrm{Ft,cold}}$ can be met with the windings $q = 2$, $W/\tau_{\mathrm{p}} = 5/6$ (fundamental winding factor $k_{\mathrm{w},1} \approx 0.933$) and $q = 3$, $W/\tau_{\mathrm{p}} = 8/9$ ($k_{\mathrm{w},1} \approx 0.945$), even for small d_{Cu}. In contrast, the $q = 2$ winding without pitching as well as the $q = 5/2$ winding require a screen with minimum thickness $d_{\mathrm{Cu,min}} \sim 8...10$ mm.

This finding, together with the restrictions on $P_{\mathrm{Ft,warm}}$, imply the use of the $q = 3$ winding in case of a sufficiently large pole pitch τ_{p} and otherwise the use of the short-pitched $q = 2$ winding. The restrictions arising from the additional

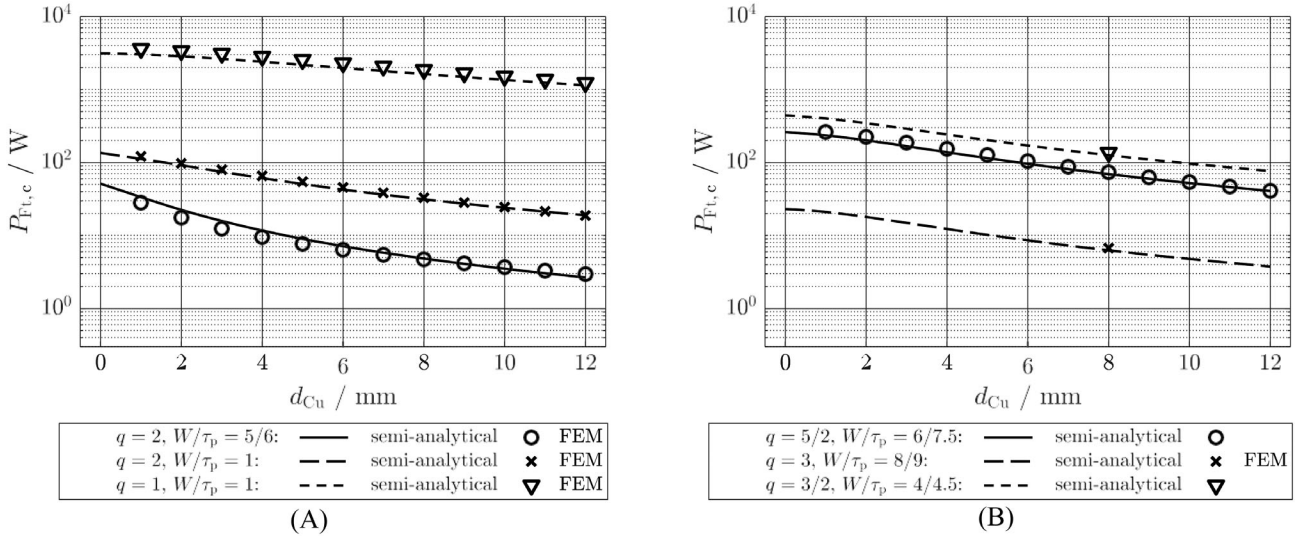

FIGURE 9 Visualisation of the eddy current loss in the cold rotor parts (rotor iron and rotor pole cores) under variation of the copper damper's thickness d_{Cu} for different stator winding configurations (A), (B). Results are shown for the 2D transient finite element method (FEM) model (JMAG 20) and the semi-analytical model.

eddy current loss, thus, imply an increase of the rotor field by more than 5%, which leads to a higher amount of HTS material and higher associated cost. In spite of the large effective air gap width, the choice of simpler stator winding configurations is, therefore, no measure to decrease the overall cost. Provided that a winding with small content of air gap field harmonics and moderate rotor field modulation is chosen, the eddy current loss can, however, be limited to an acceptable value.

4 | CONCLUSION

A semi-analytical model for the calculation of the eddy current loss in warm and cold rotor parts of HTS generators with cold rotor yoke and poles is described. The model employs a vector potential approach, where the source terms are extracted from a series of magnetostatic 2D FEM simulations. The model accounts for saturation and slot opening effects and reproduces the 2D FEM simulation results with sufficient accuracy whilst allowing for a time saving by a factor in the order of 50...100. The semi-analytical model is used to study the eddy current loss for different stator winding configurations and geometries of the damper screen and the cryostat wall. The additional loss in warm parts as well as in cold massive rotor parts are computed and the qualitative dependency on space and time order is discussed. Restrictions on the choice of the number of slots per phase and the content of air gap field harmonics are derived based on an extensive parameter study.

ACKNOWLEDGEMENTS
This work is supported by Stiftung Energieforschung Baden-Württemberg. Open Access funding enabled and organized by Projekt DEAL.

CONFLICT OF INTEREST
The authors declare no conflicts of interest.

DATA AVAILABILITY STATEMENT
The data that support the findings of this study are available from the corresponding author upon reasonable request.

ORCID
Robin Köster https://orcid.org/0000-0002-8806-8901

REFERENCES

1. Polinder H, Ferreira JA, Jensen BB, Abrahamsen AB, Atallah K, McMahon RA. Trends in wind turbine generator systems. *IEEE J Emerg Sel Top Power Electron*. 2013;1(3):174-185.
2. Song X, Bührer C, Brutsaert P, et al. Designing and basic experimental validation of the World's first MW-class direct-drive superconducting wind turbine generator. *IEEE Trans Energy Convers*. 2019;34(4):2218-2225.
3. Liu D., Polinder H., Abrahamsen A. B., Wang X., Ferreira J. A.. Comparison of superconducting generators and permanent magnet generators for 10-MW direct-drive wind turbines. International Conference on Electrical Machines and Systems (ICEMS). 2016:1–6.
4. Meeker D. C.. Finite element method magnetics, Version 4.2, 28 February 2018. https://www.femm.info. 2018.
5. Anglada JR, Sharkh SM, Yuratich MA. Calculation of rotor losses in PM machines with retaining sleeves using transfer matrices. *IET Electr Power Appl*. 2018;12(8):1150-1157.
6. Russell RL, Norsworthy KH. Eddy currents and wall losses in screened-rotor induction motors. *Proc Inst Elect Eng*. 1958;105:163-175.
7. Erd N., Köster R., Binder A.. Computational analysis of air gap field in electrical machines by Fourier coefficient matrices. International Conference on Electrical Machines (ICEM), Gothenburg, Sweden, 2020; 2020:2479–2485. 10.1109/ICEM49940.2020.9270692.
8. Stepina J. Fundamtenal equations of the space vector analysis of electrical machines. *Acta Technica CSAV*. 1968;1968(2):184-198.
9. Köster R., Binder A.. Cost-oriented design considerations on direct-drive wind turbine generators with superconducting excitation winding. International Joint Conference OPTIM–ACEMP, 2021. September, 2021.
10. Erd N., Binder A.. Eddy currents in solid rotor under spatially intermittent feeding of the stator winding. XIII International Conference on Electrical Machines (ICEM), Alexandroupoli, Greece; 2018:178–184. 10.1109/ICELMACH.2018.8507010
11. Stoll RL, Hammond P. Calculation of the magnetic field of rotating machines. Part 4: approximate determination of the field and the losses associated with eddy currents in conducting surfaces. *Proc Inst Electr Eng*. 1965;112:2083-2094.

AUTHOR BIOGRAPHIES

Robin Köster was born in 1993 near Frankfurt, Germany. He received his Master of Science in Electrical Engineering in 2018 and his Master of Science in Condensed Matter Physics from TU Darmstadt in 2020. Since 2019 he is with the Institute of Electrical Energy Conversion at the TU Darmstadt as a research assistant. His field of research are electrical machines, especially direct-drive synchronous machines for wind turbines and superconducting rotating machines.

Andreas Binder Senior Member IEEE, Member VDE, IET, VDI, EPE, received the degrees Dipl.-Ing. (diploma) and Dr. techn. (PhD) for Electrical Engineering from the University of Technology, Vienna/Austria, in 1981 and 1988, respectively. From 1981 to 1983 he worked at ELIN-Union AG, Vienna, on large synchronous generator design. From 1983 to 1989 he joined the Institute of Electrical Machines and Drives, Technical University, Vienna, as researcher. From 1989 to 1997 he rejoined industry, leading groups for developing DC and inverter-fed AC motors and drives, at Siemens AG, Bad Neustadt and Erlangen, Germany. Since 1994 he is lecturer (habilitation) at University of Technology, Vienna/Austria, and received in 1997 the ETG-Literature Award of the German Assoc. of Electrical Engineers, VDE. Since October 1997, he is Head of the Institute of Electrical Energy Conversion, Darmstadt University of Technology, as a full professor, being responsible for teaching and research for electrical machines, drives and railway systems. He is the author or co-author of more than 350 scientific publications and two books and holds several patents. He received Dr. h.c. from University of Technology Bucharest in 2007 and is the recipient of the Medal of Honour of the ETG/VDE 2009 for outstanding contributions at VDE. Research topics are High-Speed-Motors, Permanent magnet-E-Machines, bearing currents, drive technologies for hybrid and electric cars, drive systems for electric railways, magnetic suspension and magnetic bearings, generator systems.

How to cite this article: Köster R, Binder A. Eddy current loss estimation for direct drive wind turbine generators with superconducting excitation winding by numerical and analytical models. *Int J Numer Model*. 2023;36(3):e3066. doi:10.1002/jnm.3066